BULLETIN OF THE POLISH ACADEMY OF SCIENCES
TECHNICAL SCIENCES
DOI: 10.24425/bpasts.2021.136921

A New Method of Cardiac Sympathetic Index Estimation Using 1D-Convolutional Neural Network

M. KOŁODZIEJ[1], A. MAJKOWSKI[1], P. TARNOWSKI[1], R. J. RAK[1], A. RYSZ[2]

[1] Warsaw University of Technology, Institute of Theory of Electrical Engineering, Measurements and Information Systems, Warsaw, Poland
[2] Medical University of Warsaw, Department of Neurosurgery, Warsaw, Poland

Abstract. Epilepsy is a neurological disorder that causes seizures of many different types. The article presents an analysis of heart rate variability (HRV) for epileptic seizure prediction. Considering that HRV is nonstationary, our research focused on the Poincare plot feature's quantitative analysis – Cardiac Sympathetic Index (CSI). It is reported that the CSI value increases before the epileptic seizure. We proposed an algorithm using a 1D-Convolutional Neural Network (1D-CNN) for CSI estimation. The usability of this method was checked for 40 epilepsy patients. Our algorithm was compared with the method proposed by Toichi et al. The Mean Square Error (MSE) for testing data was 0.046 and Mean Absolute Percentage Error (MAPE) 0.097. The 1D-CNN algorithm was also compared with the regression methods. For this purpose, a classical type of neural network (MLP), as well as linear regression and SVM regression, were tested. In the study, typical artifacts occurring in ECG signals before and during an epileptic seizure were simulated. The proposed 1D-CNN algorithm estimates CSI well and is resistant to noise and artifacts in the ECG signal.

Key words: epilepsy, seizure detection, seizure prediction, convolutional neural network, deep learning, ECG, HRV, cardiac sympathetic index

1. Introduction

Around 50 million people worldwide have epilepsy, making it one of the most common neurological diseases globally [1]. In some cases, it is not possible to prevent epileptic seizures by using drugs or resection of the part of the cerebral cortex that is the source of seizures [2]. Certain changes in the autonomic nervous system (ANS) in people suffering from epilepsy can be observed. The change and abnormal heart rhythm are among the most important symptoms. The following changes occur before and during seizures: tachycardia, bradycardia and asystole, conduction disturbances, and heart ischemia. Their description is presented in many works [3–6]. As shown, heart rate changes are associated with sudden unexpected death (SUDEP) in patients with epilepsy. Most researchers believe that insular cortex changes lead to dysregulation of the ANS in patients with temporal lobe epilepsy (TLE).

Therefore, methods of predicting epileptic seizures are being sought. For this purpose, attempts have been made to use electrophysiological signals, in particular EEG [7–9]. The effectiveness of the developed methods is not fully satisfactory. Therefore, any additional physiological signal that can support the prediction of a seizure is valuable. In this task, attempts are made to use the ECG signal [10]. Numerous methods of quantifying heart rate variability have been proposed [11–13]. One of the features of the ECG signal is the so-called Cardiac Sympathetic Index (CSI). CSI is based on quantitative analyses of Poincare plot features. Several studies indicate that it is possible to use CSI to detect and predict seizures [14–17]. For CSI calculation, the method proposed by Toichi et al. in [18] is most often used. In our article, we use the symbolic name "Toichi" to refer to the algorithm described in this work. To determine CSI, you must first detect R waves in the ECG signal. For this purpose, you can use the well-known Pan-Tompkins algorithm [19] or another method. Next, the RR intervals should be analysed using the Poincare plot [20].

The purpose of the article is to use a 1D-Convolutional Neural Network [21–23] to calculate CSI values based on the registered ECG signal. For a trained neural network, there is no need to perform R-wave detection [24] and Poincare plot analysis. We assumed that deep learning, with many training examples from many patients, will allow the network to work effectively. The 1D-Convolutional Neural Network was used to estimate the CSI. Then we checked whether the CSI is reliable for the prediction of epileptic seizures. We also examined how the loss of part of the recorded signal or artifacts affects the calculation of the CSI using both the standard Toichi algorithm and the method we proposed. The presented research is an extension of the study described in the conference paper [25].

2. Materials

Video EEG (vEEG) with simultaneous ECG was recorded in patients with refractory temporal epilepsy for long-term monitoring of epileptic seizures during presurgical evaluation. The signals were acquired at the Medical University of Warsaw. In 40 patients who underwent epilepsy surgery in the years 2005–2015, ictal vEEG recordings provided localization information and

*e-mail: marcin.kolodziej@ee.pw.edu.pl

identification of temporal seizure type as well as ECG recordings. After noninvasive presurgical evaluation, all patients had anterior tailored lobectomy with preresection electrocorticographic recordings (iECoG). The temporal ictal onset zone was localized based on seizure ictal semiology and ictal patterns. Thirty two biosignals were registered (1 ECG channel and 31 EEG channels) using an EEG DigiTrack amplifier. The ECG signal was recorded with the sampling frequency *fs*=250Hz. For EEG registration, cup-shaped electrodes were used, and for ECG – precordial disposable electrodes located at V1 and V2 positions. During signal registration, patients were either sitting or lying, but they could freely move their heads and limbs. The registration time was from several minutes to several hours.

3. Methods

3.1 Preprocessing of ECG signal. The disturbance caused by the power line frequency (50 Hz) was removed from the ECG signal. For this purpose, a narrow-band (48-52 Hz) Butterworth digital filter was used [26, 27]. For the Toichi method, the R waves were determined in the ECG signal using the Pan and Tompkins algorithm.

3.2 Cardiac Sympathetic Index. Poincaré plots were used to analyse the nonlinear dynamics of ECG signals [28–32]. Each point in the plot is specified as n=1,2,3,…N (RR_n, RR_{n+1}), where N represents the number of recorded R waves. Such mapping reveals the correlation between consecutive RR intervals. The mapping gives useful information on short-term and long-term fluctuations of RR intervals. The mapping is shown in Figure 1, along with the standard deviation parameters *SD1* and *SD2*.

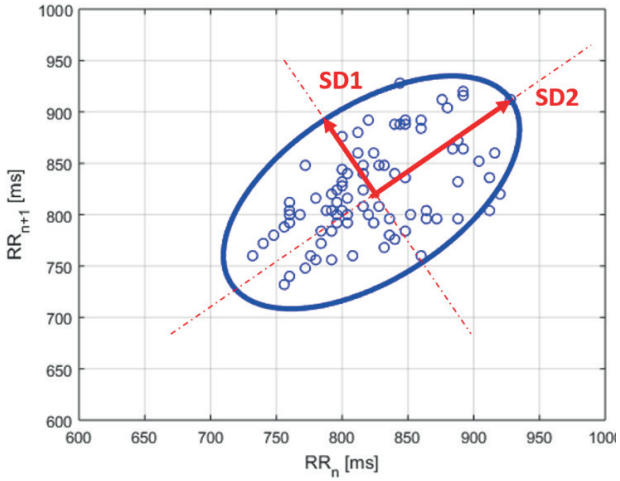

Fig. 1. Example of calculating SD1 and SD2 based on Poincaré plots.

The *SD1* shows beat-to-beat rapid changes, which are more related to respiratory sinus arrhythmia. However, *SD2* describes long-term beat-to-beat changes [33]. Cardiac Sympathetic Index *CSI=SD2/SD1* is calculated to describe the relationship between these components [18]. The *SD1* and *SD2* values in Poincaré mapping directly depend on the statistical values of the standard deviation of heart rate and two consecutive intervals of R peaks. Ellipses are described so that at least 95% of the RR data is in the ellipse area.

3.3 1D-Convolutional Neural Network. To determine the CSI value, we proposed the use of 1D-Convolutional Neural Network (1D-CNN). A one-minute ECG signal (15,000 samples) is fed to the network input, sampled at a frequency of *fs*=250 Hz (Input Layer). The network's next layers are Convolution, Batch Normalization, ReLU, MaxPooling, Dropout, Fully Connected, and Regression Output [21, 34–36]. The network structure is shown in Table 1.

Table 1
Structure of the neural network used

No.	Name of Layer	Parameters
1	Input Layer	15000 samples with zerocenter normalization
2	Conv_1	20 filters 150x1 convolutions with stride 1 and padding same
3	Batchnorm_1	Batch normalization with 20 channels
4	Relu_1	ReLU
5	Maxpool	2x1 max pooling with stride 2 and padding 0
6	Conv_2	40 filters 150x20 convolutions with stride 1 and padding same
7	Batchnorm_2	Batch normalization with 40 channels
8	Relu_2	ReLU
9	Conv_3	60 filters 10x40 convolutions with stride 1 and padding same
10	Batchnorm_3	Batch normalization with 60 channels
11	Relu_3	ReLU
12	Conv_4	60 filters 10x60 convolutions with stride 1 and padding same
13	Batchnorm_4	Batch normalization with 60 channels
14	Relu_4	ReLU
15	Conv_5	60 filters 20x60 convolutions with stride 1 and padding same
16	Batchnorm_5	Batch normalization with 60 channels
17	Relu_5	ReLU
18	Conv_6	60 filters 10x60 convolutions with stride 1 and padding same
19	Batchnorm_6	Batch normalization with 60 channels
20	Relu_6	ReLU
21	dropout	50% dropout
22	fc	1 Fully connected layer
23	Regression output	Mean-squared-error with response

The batch normalization method can be used to solve the problem of changing the distribution of hidden layer inputs [37]. This method is based on the proven property that the whitening of classifier inputs facilitates the optimization process during training. It also pays to normalize the inputs of all hidden layers in the network. Rectified Linear Unit (ReLU) is the most commonly used activation function in the field of deep learning [38]. Neural networks equipped with ReLU functions obtained better

classification accuracy than networks equipped with the hyperbolic tangent (tanh) function. Moreover, the authors of [39] found that the use of ReLU speeds up the training of the neural network four times, compared to the neural network using tanh. The most common operations that occur in the subsampling layers are MaxPooling [37]. These operations aggregate a group of adjacent samples, replacing them with samples with the maximum value. Dropout is a technique that improves the performance of neural networks across many different applications, including object classification, natural language processing, and scientific data analysis [40]. Dropout overcomes this problem by providing a way to approximately combine multiple neural networks into a single model. The method is to temporarily remove certain neurons during training. The group of neurons to be removed is selected randomly. The holding probability of a neuron is a tunable hyperparameter called the dropout rate. Neurons are drawn and removed each time a batch of samples is delivered to the network. In practice, a neuron is removed by multiplying its output by zero. The FC layer refers to a fully connected layer like in the case of a classical neural network [41].

In our research, electrocardiographic signals recorded for 40 patients were used to train CNN. Pre-seizure ECG fragments, starting ten minutes before the seizure, were selected. Windows lasting 1 minute, moved every 1 second, were used for signal analysis. In that way, 540 examples were generated for each patient. A total of 21600 examples were created for 40 patients. The data was randomly divided into three parts: 80% (17280) for training, 10% (2160) for validation, and 20% (4320) for testing.

The ADAM algorithm with the initial learning rate parameter of 0.001 was used to train the network. During training, GPU graphics processors of GeForce GTX 1070 graphics card were used. The process of training the network lasted several dozen minutes.

Figure 2 presents the procedure for the Toichi algorithm when calculating the CSI. The recorded ECG signal lasting one minute (*ECG signal*) is digitally filtered to remove the power line frequency (*Notch filter*). Then R-waves are detected in the ECG signal (*R-wave detection*). The well-known Pan and Tompkins algorithm is used for this purpose. In the next step, the time between the individual RR waves is calculated (*RR interval calculation*). The calculated RR intervals allow the computation of the Poincare plot (*Poincare plot*). Based on the Poincare plot, the SD1 and SD2 values are calculated (*SD1 and SD2 calculation*). The determined values allow the calculation of the CSI coefficient.

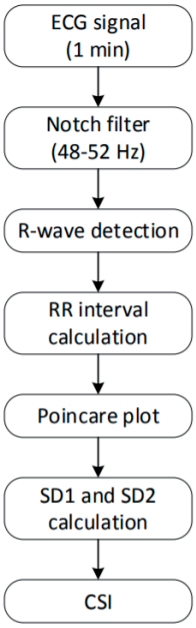

Fig. 2. CSI values calculated using the Toichi algorithm.

Figure 3 presents the procedure for the algorithm we propose using 1D-CNN. The recorded ECG signal lasting one minute (*ECG signal*) is subjected to digital filtering, the purpose of which is to remove the power line frequency – 50Hz (*Notch filter*). Then, each 1-min segment of ECG signal is fed to the input of the 1D-CNN. A trained 1D-Convolutional Neural Network calculates the CSI.

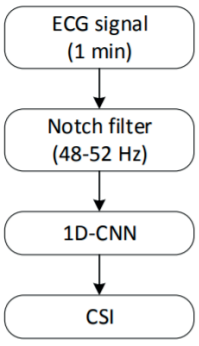

Fig. 3. CSI values calculated using the 1D-CNN.

4. Results and discussion

To prevent overfitting of the neural network, a validation set was used. An expert verified all examples used for training, validation, and testing to assess the correct R-wave detection. The proposed by Toichi et al. CSI calculation method was considered as the reference – showing the correct values.

The difference between the estimations of the CSI value calculated using the Toichi algorithm and the 1D-Convolutional Neural Network was calculated. We

calculated Mean Squared Error (equal 0.046) and Mean Absolute Percentage Error (0.097) for the testing set as a measure of the difference. Additionally, to determine the correctness of the CSI estimation, the maximum, minimum, and average values of this index were calculated using both algorithms. The maximum CSI value calculated using the Toichi algorithm was 7.873 while using 1D-CNN – 7.324. The minimum CSI value calculated using the Toichi algorithm was 1.001 while using 1D-CNN – 0.092. The average CSI value calculated using the Toichi algorithm was 1.956 while using 1D-CNN – 1.849. The obtained results proved the correct estimation of the CSI value by 1D-CNN.

Figure 4 presents an example of the calculated CSI values with the Toichi and 1D-CNN algorithms for one of the patients. We can observe significant fluctuations in CSI values. Although the CSI values calculated using the Toichi method slightly differ from these calculated using 1D-CNN, there is a large correlation between them, $\rho = 0.97$.

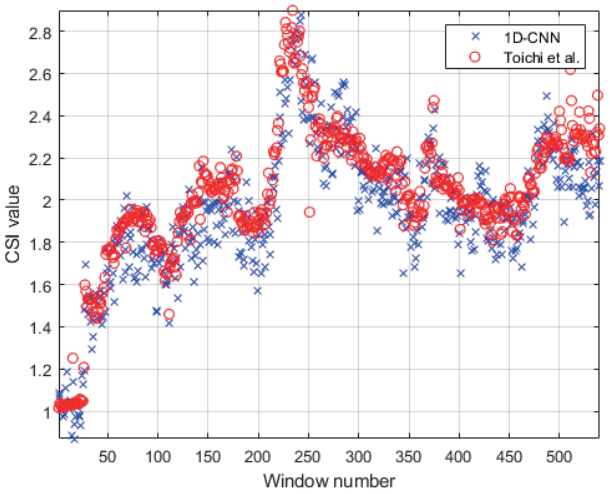

Fig. 4. CSI values calculated using the Toichi and 1D-CNN algorithms.

Figure 5 presents the RR interval variability for subsequent heartbeats. We can observe significant variation in the RR interval. Figure 6 shows Poincare plots for one patient for an ECG signal registered 10 minutes before the seizure (blue) and one minute before the seizure (red). For this patient, the CSI value calculated using the Toichi algorithm was 1.535 for ten minutes before the seizure and 2.417 for one minute before the seizure. In contrast, the CSI value estimated using 1D-CNN was 1.549 for ten minutes before the seizure and 2.018 for one minute before the seizure.

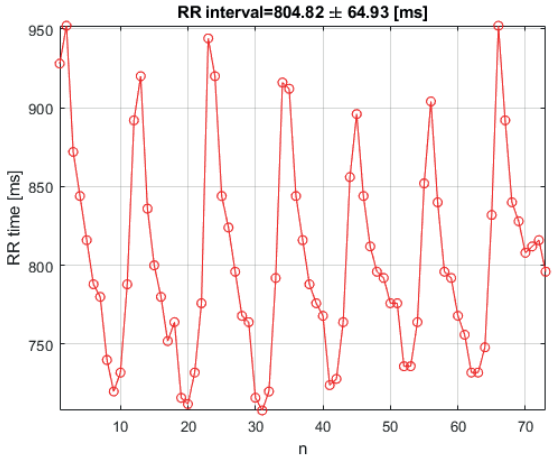

Fig. 5. Example of RR interval variation for the signal one minute before the seizure.

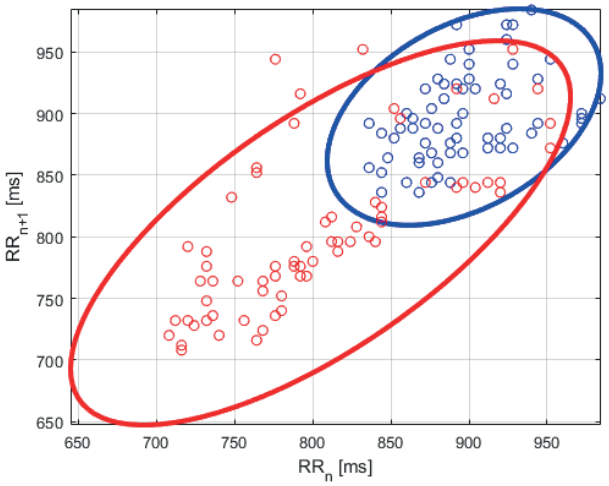

Fig. 6. Poincaré plots for one patient 10 minutes before the seizure (blue) and one minute before the seizure (red).

We also examined the influence of disturbances that may occur during the registration of ECG signals on the CSI estimation error. For this purpose, a one-minute ECG signal recording was chosen, with correctly detected R waves. The standard deviation for the selected ECG signal samples was $\sigma = 0.928$. CSIs were calculated using the Toichi and 1D-CNN algorithms. Then, signal fragments (from 0.5 to 20 seconds) were removed from the center of the ECG waveform, and CSI values were calculated again using the Toichi algorithm and 1D-CNN. Such removal of the signal was intended to simulate the artifact of the temporary disconnection of the ECG electrode. Figure 7 shows the ECG signal fragment with the simulated removal of 8 seconds of the signal.

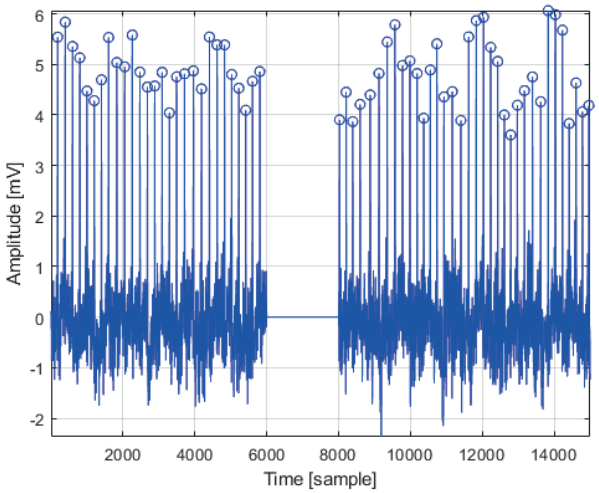

Fig. 7. A fragment of the ECG signal with the removal of 8 seconds of the signal.

In the next stage, the ECG signal was disturbed by noise with a normal distribution and amplitude of 0.5σ, 1σ, 1.5σ, and 2σ of the standard deviation of the ECG waveform. In this case, the signal noise was intended to simulate low-amplitude long-term EMG artifacts. Then the ECG signal was disturbed by noise with a normal distribution and amplitude from 2σ to 6σ times greater than the ECG signal's standard deviation. The duration of the signal disturbance ranged from 2 to 4 seconds. This signal noise was intended to simulate high-amplitude short-term EMG artifacts. An example of such an artifact is presented in Fig. 8.

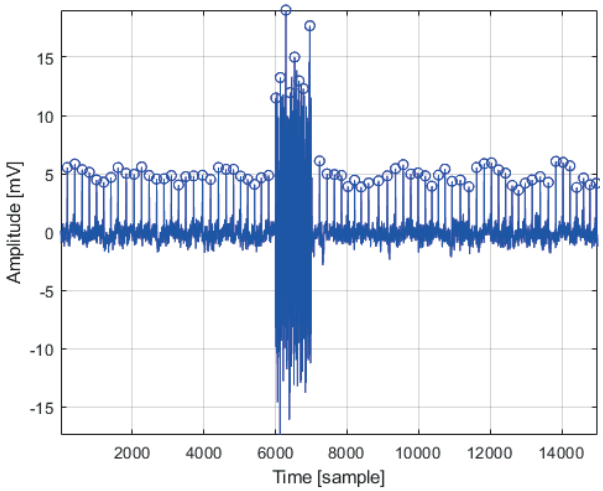

Fig. 8. A fragment of ECG signal with 4-second EMG artifact.

Finally, the influence of sinusoidal disturbances was examined. Such kind of disturbance simulates floating electrode artifacts. For this purpose, a sinusoidal signal with amplitude 1 and frequencies from 0.05 Hz to 10 Hz was added to the ECG signal. An example of a disturbed signal with a sinusoidal artifact is presented in Fig. 9.

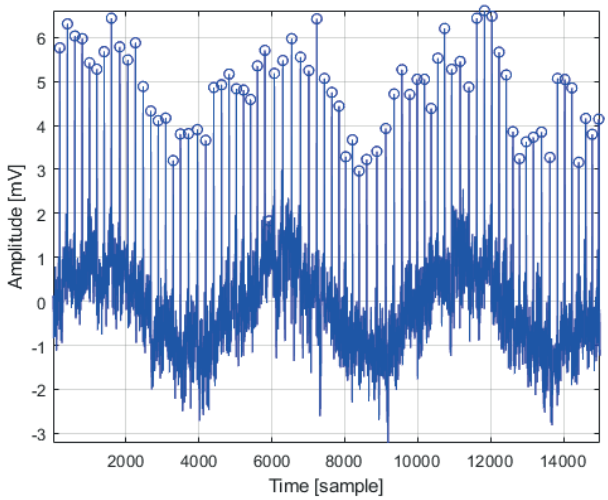

Fig. 9. A fragment of ECG signal with a floating electrode artifact.

Then CSI was calculated for each case using the Toichi and 1D-CNN algorithms. The calculated CSI values for the loss of ECG signal fragments are presented in Table 2. For each calculated CSI value, an error was determined, that is, the difference between the calculated CSI value for the disturbed signal and the CSI value calculated for the undisturbed signal using the Toichi algorithm.

Table 2
CSI values for loss of fragments of ECG signal

Loss of signal	Toichi et al.		1D-CNN	
	CSI	Error	CSI	Error
Undisturbed	2.200	-	2.196	0.004
20 sec	1.101	1.099	2.037	0.163
10 sec	1.012	1.188	2.283	-0.083
4 sec	1.026	1.174	2.355	-0.155
2 sec	1.096	1.104	2.176	0.024
1 sec	1.265	0.935	2.152	0.048
0.5 sec	1.265	0.935	2.112	0.088

The proposed 1D-CNN algorithm estimates the CSI values much more accurately than the Toichi algorithm. Even for a loss of 20 seconds of the ECG signal, the CSI estimation's correctness is acceptable. Table 3 presents the calculated CSI values for floating electrode artifacts.

Table 3
CSI values for floating electrode artifacts

Sinusoidal signal	Toichi et al.		1D-CNN	
	CSI	Error	CSI	Error
Undisturbed	2.200	-	2.196	0.004
0.05Hz	1.920	0.280	2.233	-0.033
0.1Hz	1.923	0.277	2.249	-0.049
0.2Hz	1.607	0.593	2.223	-0.023
1Hz	1.956	0.244	1.092	1.108
10Hz	1.792	0.408	3.471	-1.271

For the ECG signal disturbed by a sinusoidal waveform with frequencies from 0.05 Hz to 0.2 Hz, we obtain a more accurate estimation of the CSI value using the proposed

1D-CNN algorithm than with the Toichi algorithm. Worse results of the CSI coefficient approximation were obtained for the sinusoidal signal in the range of 1 Hz to 10 Hz.

Table 4 presents the results of the calculated CSI values for ECG signal with added noise of normal distribution (simulated EMG artifacts). For the noise values from 0.5σ to 1.5σ, we obtain a more accurate estimation of the CSI value using the proposed 1D-CNN algorithm than with the Toichi algorithm. However, for a disturbance with an amplitude of 2σ, it happened in one case that the value of the CSI coefficient determined by the Toichi algorithm was more accurate.

Table 4
CSI values for ECG signal with simulated low-amplitude long-term EMG artifacts

Normal distribution noise	Toichi et al.		1D-CNN	
	CSI	Error	CSI	Error
Undisturbed	2.200	-	2.196	0.004
0.5σ	1.781	0.419	2.193	0.007
0.5σ	1.904	0.296	2.347	-0.147
0.5σ	1.616	0.584	2.103	0.097
1σ	1.220	0.98	2.403	-0.203
1σ	1.159	1.041	2.191	0.009
1σ	1.609	0.591	2.150	0.050
1.5σ	1.166	1.034	1.577	0.623
1.5σ	1.532	0.668	1.937	0.263
1.5σ	1.286	0.914	2.047	0.153
2σ	1.391	0.809	1.930	0.270
2σ	1.404	0.796	1.206	0.994
2σ	1.175	1.025	1.974	0.226

Table 5 presents the results of CSI value estimation for ECG signal with 2 seconds high-amplitude EMG artifacts. For the disturbance amplitude from 2σ to 6σ, again, the 1D-CNN algorithm gave better results than the Toichi algorithm. The presented results indicate that the 1D-CNN algorithm is more robust to artifacts specific to the ECG signal recordings.

Table 5
CSI values for ECG with simulated high-amplitude short-term EMG artifacts

Normal distribution noise	Toichi et al.		1D-CNN	
	CSI	Error	CSI	Error
Undisturbed	2.200	-	2.196	0.004
2σ	1.440	0.760	2.248	-0.048
2σ	1.332	0.868	2.177	0.023
2σ	1.065	1.135	2.238	-0.038
4σ	1.611	0.589	2.072	0.128
4σ	1.645	0.555	2.142	0.058
4σ	1.588	0.612	2.065	0.135
6σ	1.259	0.941	2.022	0.178
6σ	1.071	1.129	2.077	0.123
6σ	1.765	0.435	2.071	0.129

The CSI calculation time for one minute of ECG signal was tested using the Toichi and 1D-CNN algorithms. The average calculation time for 1D-CNN was 0.0048 seconds, while for Toichi – 0.0029. For both algorithms, the CSI calculation time is comparable and can be used in practice.

We also checked whether an advanced neural network (1D-CNN) is really needed to approximate the CSI coefficient. For this purpose, we compared the performance of MLP with one hidden layer with the results obtained for 1D-CNN. During the research, we changed the number of neurons in the hidden layer. The Levenberg-Marquardt algorithm was used to train the MLP. The same data was used for MLP and 1D-CNN: 17280 examples were used for training, 2160 for validation, and 4320 for testing. Table 6 presents the mean squared errors for a particular number of neurons in the hidden layer of MLP. The obtained results indicate that the proposed 1D-CNN allows for a much more accurate estimation of the CSI values. The smallest MSE error (0.637) for the MLP was obtained for 300 neurons in the hidden layer. This is an order of magnitude more than for the 1D-CNN.

Table 6
MSE error comparison for MLP and 1D-CNN

Neural network	Number of neurons in the hidden layer	MSE
MLP	1000	0.704
MLP	500	1.600
MLP	300	0.637
MLP	100	0.726
MLP	50	0.667
MLP	10	0.804
1D-CNN	**-**	**0.046**

The performance of the 1D-CNN was also compared with other regression methods. Two algorithms, Linear Regression and SVM Regression (quadratic kernel) were selected for comparison. The PCA method was used to reduce the input data set. For this purpose, components explaining 95% of the variance of the set were selected. The same data was used for regression and for 1D-CNN training and testing. Table 7 presents the MSE errors for the testing set for individual regression methods. Again, the MSE error for 1D-CNN is an order of magnitude smaller.

Table 7
MSE error for the regression and 1D-CNN methods

Regression method	MSE
PCA+Linear Regression	0.878
PCA+SVM Regresion	0.860
1D-CNN	**0.046**

Figure 10a presents an exemplary 5-second segment of the ECG signal fed to the input of the 1D-CNN and three exemplary ECG signals after passing through the network's digital filters of the first convolutional layer (Fig. 10b,c,d). The interpretation of the received signals is difficult. However, for the third signal (Fig. 10d), we can observe the effective "extraction" of R waves. Further layers of the neural network use the created filters to calculate new features and, as a result, to calculate the CSI.

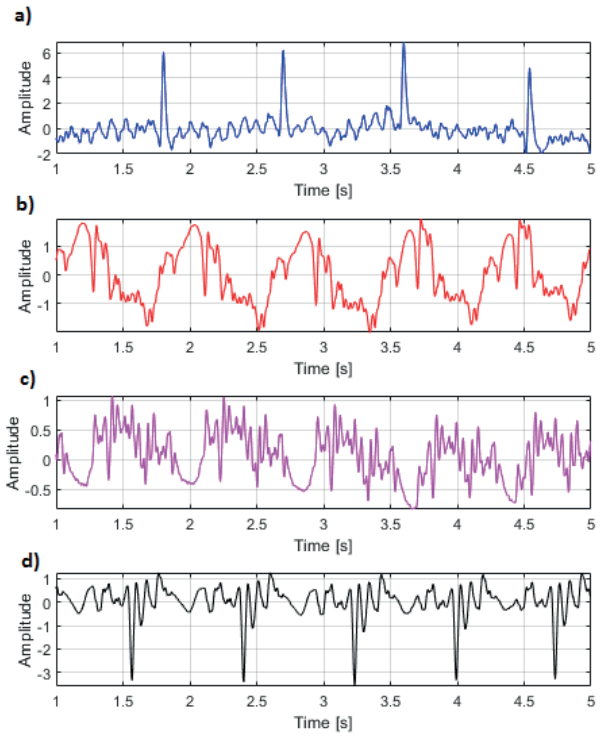

Fig. 10. (a) An example of a 5-second segment of the ECG signal fed to the neural network's input and the exemplary signals after the different filters created by the first layer of 1D-CNN, (b) filter number one, (c) filter number two, (d) filter number three.

In another experiment, the influence of the size of the first convolution layer of 1D-CNN on the accuracy of the obtained results was checked. Table 8 shows the MSE error for sample filter size (50, 150, 300, and 500). In each case, very similar MSE error values were obtained. However, the best results were obtained with a filter size of 150.

Table 8
Comparison of the MSE error for 1D-CNN for different filter sizes of the first convolution layer

Filter size	50	**150**	300	500
MSE	0.049	**0.046**	0.056	0.064

To emphasize the purposefulness of the conducted research, it was additionally checked whether there is a chance of using CSI to predict or detect an epileptic seizure. CSI variability was calculated using the Toichi and 1D-CNN algorithms for each user. Then the result obtained for each of the 40 users was averaged. Figure 11 presents the average value of CSI for the Toichi and 1D-CNN algorithms 9 minutes before an epileptic seizure. For CSI calculated using Toichi and 1D-CNN, we can observe a significant increase about a minute before the seizure.

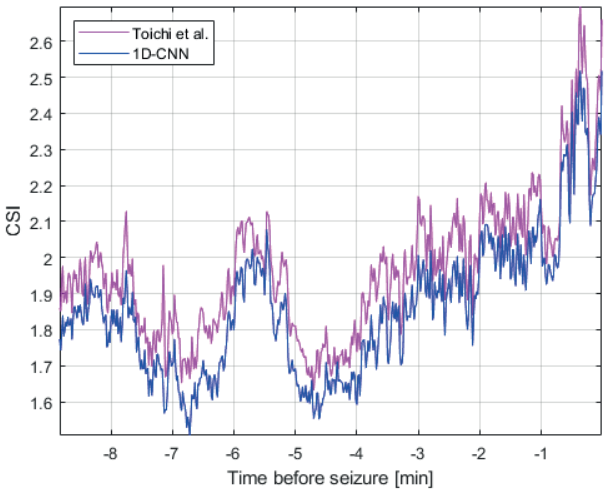

Fig. 11. CSI values averaged for 40 people for the Toichi and 1D-CNN algorithms 9 minutes before the epileptic seizure.

The mean preseizure CSI value for 1D-CNN is 2.205 and for the Toichi algorithm is 2.300 (the difference is 4.3%). We can observe higher CSI values determined using the Toichi algorithm than 1D-CNN. Figure 12 shows the statistical distribution of CSI values calculated using the Toichi algorithm and 1D-CNN. Using both the Toichi and CNN methods, we are able to indicate a statistically significant increase (p <0.001) of the CSI value a minute before the seizure.

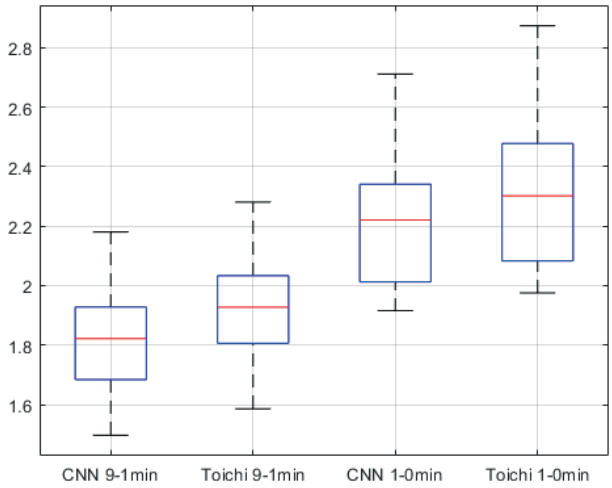

Fig. 12. Boxplot of CSI values calculated using Toichi and 1D-CNN algorithm for 9 to 1 and 1 to 0 minutes before the seizure.

This confirms the assumption that, in general, there is an increase in CSI before epileptic seizures. However, to assess the effectiveness of such a prediction method, further research is required regarding CSI variability over a longer period of time. This is outside the scope of this work.

5. Conclusions

The proposed structure of the 1D-CNN allows for an effective approximation of the Cardiac Sympathetic Index. Mean Squared Error is MSE=0.046 and Mean Absolute Percentage Error MAPE=0.097. The solution we propose, based on 1D-CNN, allows for a better estimation of the Cardiac Sympathetic Index than other regression methods and is more resistant to various types of disturbances. Unfortunately, training a 1D-CNN requires many examples from many people, and the ECG data must be of good quality. The use of 1D-CNN for CSI calculations is more reliable for an ECG signal containing disturbances that may occur during ECG signal registration, especially during an epileptic seizure. The CSI variability indicates that there is a chance to use the ECG signal to predict or detect an epileptic seizure.

References

[1] World Health Organization (WHO), "Epilepsy," Jun. 2019. Accessed: Jul. 10, 2020. [Online]. Available: https://www.who.int/news-room/fact-sheets/detail/epilepsy.

[2] B. Sommer *et al.*, "Resection of cerebral gangliogliomas causing drug-resistant epilepsy: short- and long-term outcomes using intraoperative MRI and neuronavigation," *Neurosurgical Focus*, vol. 38, no. 1, p. E5, Jan. 2015, doi: 10.3171/2014.10.FOCUS14616.

[3] T. Harnod, C. C. H. Yang, Y.-L. Hsin, P.-J. Wang, K.-R. Shieh, and T. B. J. Kuo, "Heart rate variability in patients with frontal lobe epilepsy," *Seizure*, vol. 18, no. 1, pp. 21–25, Jan. 2009, doi: 10.1016/j.seizure.2008.05.013.

[4] K. Jansen and L. Lagae, "Cardiac changes in epilepsy," *Seizure*, vol. 19, no. 8, pp. 455–460, Oct. 2010, doi: 10.1016/j.seizure.2010.07.008.

[5] R. Brotherstone and A. McLellan, "Parasympathetic alteration during sub-clinical seizures," *Seizure*, vol. 21, no. 5, pp. 391–398, Jun. 2012, doi: 10.1016/j.seizure.2012.03.011.

[6] A. Van de Vel *et al.*, "Non-EEG seizure detection systems and potential SUDEP prevention: State of the art: Review and update," *Seizure*, vol. 41, pp. 141–153, Oct. 2016, doi: 10.1016/j.seizure.2016.07.012.

[7] U. R. Acharya, Y. Hagiwara, and H. Adeli, "Automated seizure prediction," *Epilepsy Behav*, vol. 88, pp. 251–261, 2018, doi: 10.1016/j.yebeh.2018.09.030.

[8] G. Giannakakis, V. Sakkalis, M. Pediaditis, and M. Tsiknakis, "Methods for Seizure Detection and Prediction: An Overview," in *Modern Electroencephalographic Assessment Techniques: Theory and Applications*, V. Sakkalis, Ed. New York, NY: Springer, 2015, pp. 131–157.

[9] E. Bou Assi, D. K. Nguyen, S. Rihana, and M. Sawan, "Towards accurate prediction of epileptic seizures: A review," *Biomedical Signal Processing and Control*, vol. 34, pp. 144–157, Apr. 2017, doi: 10.1016/j.bspc.2017.02.001.

[10] G. Giannakakis, M. Tsiknakis, and P. Vorgia, "Focal epileptic seizures anticipation based on patterns of heart rate variability parameters," *Computer Methods and Programs in Biomedicine*, vol. 178, pp. 123–133, Sep. 2019, doi: 10.1016/j.cmpb.2019.05.032.

[11] M. Kotas, "Projective filtering of time-aligned beats for foetal ECG extraction," *Bulletin of the Polish Academy of Sciences: Technical Sciences*, vol. 55, no. 4, 2007.

[12] K. Lewenstein, M. Jamroży, and T. Leyko, "The use of recurrence plots and beat recordings in chronic heart failure detection," *Bulletin of the Polish Academy of Sciences: Technical Sciences*, vol. 64, no. No 2, pp. 339–345, 2016.

[13] J. Jarczewski, A. Furgała, A. Winiarska, M. Kaczmarczyk, and A. Poniatowski, "Cardiovascular response to different types of acute stress stimulations," *Folia Medica Cracoviensia*, vol. 59, no. No 4, pp. 95–110, Dec. 2019.

[14] J. Jeppesen, S. Beniczky, P. Johansen, P. Sidenius, and A. Fuglsang-Frederiksen, "Comparing maximum autonomic activity of psychogenic non-epileptic seizures and epileptic seizures using heart rate variability," *Seizure*, vol. 37, pp. 13–19, Apr. 2016, doi: 10.1016/j.seizure.2016.02.005.

[15] J. Jeppesen, S. Beniczky, P. Johansen, P. Sidenius, and A. Fuglsang-Frederiksen, "Detection of epileptic seizures with a modified heart rate variability algorithm based on Lorenz plot," *Seizure*, vol. 24, pp. 1–7, Jan. 2015, doi: 10.1016/j.seizure.2014.11.004.

[16] J. Jeppesen, S. Beniczky, P. Johansen, P. Sidenius, and A. Fuglsang-Frederiksen, "Using Lorenz plot and Cardiac Sympathetic Index of heart rate variability for detecting seizures for patients with epilepsy," in *2014 36th Annual International Conference of the IEEE Engineering in Medicine and Biology Society*, Aug. 2014, pp. 4563–4566, doi: 10.1109/EMBC.2014.6944639.

[17] F. Fürbass *et al.*, "Automatic multimodal detection for long-term seizure documentation in epilepsy," *Clinical Neurophysiology*, vol. 128, no. 8, pp. 1466–1472, Aug. 2017, doi: 10.1016/j.clinph.2017.05.013.

[18] M. Toichi, T. Sugiura, T. Murai, and A. Sengoku, "A new method of assessing cardiac autonomic function and its comparison with spectral analysis and coefficient of variation of R-R interval," *J. Auton. Nerv. Syst.*, vol. 62, no. 1–2, pp. 79–84, Jan. 1997, doi: 10.1016/s0165-1838(96)00112-9.

[19] J. Pan and W. J. Tompkins, "A Real-Time QRS Detection Algorithm," *IEEE Transactions on Biomedical Engineering*, vol. BME-32, no. 3, pp. 230–236, Mar. 1985, doi: 10.1109/TBME.1985.325532.

[20] S. Rezaei, S. Moharreri, S. Ghiasi, and S. Parvaneh, "Diagnosis of sleep apnea by evaluating points distribution in poincare plot of RR intervals," in *2017 Computing in Cardiology (CinC)*, Sep. 2017, pp. 1–4, doi: 10.22489/CinC.2017.158-398.

[21] S. Kiranyaz, O. Avci, O. Abdeljaber, T. Ince, M. Gabbouj, and D. J. Inman, "1D Convolutional Neural Networks and Applications: A Survey," *arXiv:1905.03554 [cs, eess]*, May 2019, Accessed: Jul. 10, 2020. [Online]. Available: http://arxiv.org/abs/1905.03554.

[22] T. Poggio and Q. Liao, "Theory I: Deep networks and the curse of dimensionality," *Bulletin of the Polish Academy of Sciences: Technical Sciences*, vol. 66, no. No 6 (Special Section on Deep Learning: Theory and Practice), pp. 761–773, Dec. 2018.

[23] J. Kurek, B. Świderski, S. Osowski, M. Kruk, and W. Barhoumi, "Deep learning versus classical neural approach to mammogram recognition," *Bulletin of the Polish Academy of Sciences: Technical Sciences*, vol. Vol. 66, no. nr 6, 2018, doi: 10.24425/bpas.2018.125930.

[24] Y. Zhang and Z. Wang, "Research on intelligent algorithm for detecting ECG R waves," in *2015 IEEE 5th International Conference on Electronics Information and Emergency Communication*, May 2015, pp. 47–50, doi: 10.1109/ICEIEC.2015.7284484.

[25] M. Kołodziej, A. Majkowski, P. Tarnowski, R. J. Rak, and A. Rysz, "Implementation of 1DConvolutional Neural Network for Cardiac Sympathetic Index Estimation," presented at the 2020 IEEE 21st International Conference on Computational Problems of Electrical Engineering (CPEE), 2020.

[26] K. M. Gaikwad and M. S. Chavan, "Removal of high frequency noise from ECG signal using digital IIR butterworth filter," in *2014 IEEE Global Conference on Wireless Computing Networking (GCWCN)*, Dec. 2014, pp. 121–124, doi: 10.1109/GCWCN.2014.7030861.

[27] M. Kołodziej, A. Majkowski, and R. J. Rak, "A new method of feature extraction from EEG signal for brain-computer interface design," *Przeglad Elektrotechniczny*, vol. 9, pp. 35–38, 2010.

[28] K. Hayase, K. Hayashi, and T. Sawa, "Hierarchical Poincaré analysis for anaesthesia monitoring," *J Clin Monit Comput*, Dec. 2019, doi: 10.1007/s10877-019-00447-0.

[29] J. Niehoff, M. Matzkies, F. Nguemo, J. Hescheler, and M. Reppel, "The Effect of Antiarrhythmic Drugs on the Beat Rate Variability of Human Embryonic and Human Induced Pluripotent Stem Cell Derived Cardiomyocytes," *Sci Rep*, vol. 9, no. 1, p. 14106, Oct. 2019, doi: 10.1038/s41598-019-50557-7.

[30] M. M. Platiša, T. Bojić, S. Mazić, and A. Kalauzi, "Generalized Poincaré plots analysis of heart period dynamics in different physiological conditions: Trained vs. untrained men," *PLoS ONE*, vol. 14, no. 7, p. e0219281, 2019, doi: 10.1371/journal.pone.0219281.

[31] P. Fontana *et al.*, "Applicability of a Textile ECG-Belt for Unattended Sleep Apnoea Monitoring in a Home Setting," *Sensors (Basel)*, vol. 19, no. 15, Jul. 2019, doi: 10.3390/s19153367.

[32] T. Schmidt, S. Wulff, K.-M. Braumann, and R. Reer, "Determination of the Maximal Lactate Steady State by HRV in Overweight and Obese Subjects," *Sports Med Int Open*, vol. 3, no. 2, pp. E58–E64, Apr. 2019, doi: 10.1055/a-0883-5473.

[33] J. Piskorski and P. Guzik, "Geometry of the Poincaré plot of RR intervals and its asymmetry in healthy adults," *Physiol Meas*, vol. 28, no. 3, pp. 287–300, Mar. 2007, doi: 10.1088/0967-3334/28/3/005.

[34] Ö. Yıldırım, P. Pławiak, R.-S. Tan, and U. R. Acharya, "Arrhythmia detection using deep convolutional neural network with long duration ECG signals," *Computers in Biology and Medicine*, vol. 102, pp. 411–420, Nov. 2018, doi: 10.1016/j.compbiomed.2018.09.009.

[35] B. Zhao, H. Lu, S. Chen, J. Liu, and D. Wu, "Convolutional neural networks for time series classification," *Journal of Systems Engineering and Electronics*, vol. 28, no. 1, pp. 162–169, Feb. 2017, doi: 10.21629/JSEE.2017.01.18.

[36] V. Lebedev and V. Lempitsky, "Speeding-up convolutional neural networks: A survey," *Bulletin of the Polish Academy of Sciences: Technical Sciences*, vol. 66, no. 6, 2018, doi: 10.24425/BPAS.2018.125927.

[37] M. Grochowski, A. Kwasigroch, and A. Mikołajczyk, "Selected technical issues of deep neural networks for image classification purposes," *Bulletin of the Polish Academy of Sciences: Technical Sciences*, vol. 67, no. No. 2, pp. 363–376, Apr. 2019.

[38] Xavier Glorot, Antoine Bordes, and Yoshua Bengio, "Deep Sparse Rectifier Neural Networks," in *Proceedings of the Fourteenth International Conference on Artificial Intelligence and Statistics*, Jun. 2011, pp. 315–323, [Online]. Available: http://proceedings.mlr.press/v15/glorot11a.html.

[39] A. Krizhevsky, I. Sutskever, and G. E. Hinton, "ImageNet classification with deep convolutional neural networks," *Commun. ACM*, vol. 60, no. 6, pp. 84–90, May 2017, doi: 10.1145/3065386.

[40] Y. Gal and Z. Ghahramani, "A Theoretically Grounded Application of Dropout in Recurrent Neural Networks," in *Advances in Neural Information Processing Systems 29*, D. D. Lee, M. Sugiyama, U. V. Luxburg, I. Guyon, and R. Garnett, Eds. Curran Associates, Inc., 2016, pp. 1019–1027.

[41] S. Albawi, T. A. Mohammed, and S. Al-Zawi, "Understanding of a convolutional neural network," in *2017 International Conference on Engineering and Technology (ICET)*, Aug. 2017, pp. 1–6, doi: 10.1109/ICEngTechnol.2017.8308186.